



# Fabrication and investigation on Ag nanowires/TiO<sub>2</sub> nanosheets/graphene hybrid nanocomposite and its water treatment performance

Chao Liu<sup>1</sup> · Yang Lin<sup>1</sup> · Yufei Dong<sup>2</sup> · Yingke Wu<sup>2</sup> · Yan Bao<sup>2</sup> · Hongxia Yan<sup>3</sup> · Jianzhong Ma<sup>2</sup>

Received: 21 January 2020 / Revised: 22 April 2020 / Accepted: 20 June 2020 / Published online: 29 June 2020  
© Springer Nature Switzerland AG 2020

## Abstract

In this paper, a novel Ag nanowires/TiO<sub>2</sub> nanosheets/graphene nanocomposite was fabricated via a facile method of hydrothermal and calcination, and then the water treatment performance of it was evaluated for methylene blue (MB) and *Escherichia coli* removal. The as-prepared Ag nanowires/TiO<sub>2</sub> nanosheets/graphene nanocomposite was characterized by Fourier-transform infrared spectroscopy (FT-IR), X-ray photoelectron spectroscopy (XPS), X-ray diffraction (XRD), field-emission scanning electron microscopy (FE-SEM), energy-dispersive X-ray spectroscopy (EDX), UV–visible diffuse reflection spectroscopy (DRS), molecular dynamics simulation, and gas chromatography–mass spectrometry (GC-MS). All data revealed that the Ag/TiO<sub>2</sub>/graphene nanocomposite showed a rich cell structure. The photocatalytic activity of Ag/TiO<sub>2</sub>/graphene nanocomposite is higher than those of pristine TiO<sub>2</sub> nanosheets and TiO<sub>2</sub>/graphene nanocomposite. Under optimized conditions, the degradation efficiency was 100% and 71% for MB (30 mg/L) and with 10 mg Ag/TiO<sub>2</sub>/graphene nanocomposite under UV and visible light irradiation for 2 h, respectively. Ag/TiO<sub>2</sub>/graphene also showed excellent bacteria-killing activity. Meanwhile, the Ag/TiO<sub>2</sub>/graphene nanocomposite exhibited microstructure stability and cyclic stability. The water treatment performance was enhanced mainly attributed to the excellent adsorption performance of graphene and the high efficiency in separation of electron–hole pairs induced by the remarkable synergistic effects of TiO<sub>2</sub>, Ag, and graphene. On the basis of the experimental results, the photocatalytic mechanism and MB degradation mechanism were proposed. It is hoped that our work could avert the misleading message to the readership, hence offering a valuable source of reference on fabricating composite photocatalyst with stable microstructure and excellent performance for their application in the environment clean-up.

**Keywords** TiO<sub>2</sub> nanosheet · Graphene · Ag nanowire · Adsorption · Photocatalytic · Molecular dynamics simulation

**Electronic supplementary material** The online version of this article (<https://doi.org/10.1007/s42114-020-00164-2>) contains supplementary material, which is available to authorized users.

✉ Chao Liu  
lc1010158@163.com

<sup>1</sup> Shaanxi Collaborative Innovation Center of Industrial Auxiliary Chemistry and Technology, Shaanxi University of Science & Technology, Xi'an 710021, China

<sup>2</sup> College of Bioresources Chemical and Materials Engineering, Shaanxi University of Science & Technology, Xi'an 710021, China

<sup>3</sup> Key Laboratory of Space Applied Physics and Chemistry, Ministry of Education, Department of Applied Chemistry, School of Science, Northwestern Polytechnical University, Xi'an 710129, China

## 1 Introduction

Titanium dioxide (TiO<sub>2</sub>) has been regarded as one of the most attractive photocatalyst in environmental remediation because of its non-toxicity, low cost, and chemical stability [1–3]. However, the high recombination rate of photo-generated electron–hole pairs greatly reduces its photocatalytic activity. Besides, it has a wide band gap and requires UV irradiation, which greatly reduces its practical value [4, 5]. What is more, nanometer-sized TiO<sub>2</sub> is easy to agglomerate in a solution. Thus, inhibition of photo-generated electron–hole pair recombination, extending light absorption into the visible light region, and inhibiting agglomeration are three key methods to improve the photocatalytic activity of TiO<sub>2</sub> under visible light irradiation [6, 7].

There are various carbon materials that play an important role in multiphase catalysis as catalysts or carriers. As a novel

two-dimensional carbon nanomaterial, graphene has attracted great attention due to its incredible self-lubrication, high electrical conductivity, outstanding thermal conductivity, and high specific surface area [8–12]. Most aromatic pollutants can be easily adsorbed on graphene surface due to  $\pi$ - $\pi$  stacking effect [13, 14]. Therefore, many researchers have prepared high-efficiency photocatalyst/graphene composites by depositing a photocatalyst on the surface of graphene [15–17]. The outstanding photocatalytic performance is mainly because the existence of graphene can not only enhance the adsorption capacity of photocatalyst but also reduce the recombination of photo-generated electron–hole pairs [18]. Meanwhile, noble metal materials, especially Ag, have attracted great attention from researchers due to their good antibacterial, optical, and catalytic properties [19–22]. Ag can not only transfer photo-generated electrons to reduce the recombination ratio of photo-generated electron–hole pairs but can also exhibit local surface plasmon resonance (LSPR) phenomenon, which makes the composite catalysts have strong and wide absorption in the visible light region. However, graphene nanosheets and Ag nanoparticles are also easy to aggregate, which is not conducive to its practical application. In addition, the interaction between the photocatalytic materials and graphene or Ag nanoparticles determines the separation ability of photo-generated electrons and holes, and the microstructure stability of composite photocatalyst [23, 24]. So, the morphology of the photocatalytic materials may affect the photocatalytic performance, reusability, and biosecurity of photocatalyst/graphene composites for their application in the water treatment. It is of great significance to promote the practical application of nanomaterials to assemble macroscopic structures with nanomaterials while maintaining their original properties and interaction strength. Recently, we find that a new type of three-dimensional (3D) graphene foam can not only avoid the stack of graphene nanosheets and effectively maintain its large specific surface area but also can minimize the reflection of incident light and improve the efficiency of light utilization [25, 26]. Meanwhile, it can be easily separated and recovered. Therefore, more and more researches have been done to fabricate various 3D graphene composites [27, 28]. The photocatalytic degradation efficiency can be effectively improved by introducing photocatalyst into surface of the foam scaffold [29, 30]. Such composite foams are likely to be ideal candidates as treatment agents for light-driven environmental restoration, while the stability of foam structure largely determines the durability of its performance.

To the best of our knowledge, there has been no research concerning Ag nanowires/TiO<sub>2</sub> nanosheets/graphene nanocomposite used as water treatment materials. In this work, novel 3D Ag nanowires/TiO<sub>2</sub> nanosheets/graphene nanocomposite was synthesized and used as an efficient water treatment agent for removing methylene blue (MB) and *Escherichia coli*. Then, the adsorption and photocatalytic

performances of the prepared nanocomposite were investigated. Further, the microstructure stability of it was studied by molecular dynamics simulation method under COMPASS force fields. Finally, its adsorption and photocatalytic mechanism were proposed.

## 2 Materials and methods

### 2.1 Materials

For nanocomposite preparation, graphite natural powder (325 mesh) was purchased from Alfa Aesa. Butyl titanate was purchased from Tianjin Kermel Chemistry Co., Ltd. Hydrofluoric acid (HF, 40%), methylene blue (MB), and 2-(2-methoxy-4-nitrophenyl)-3-(4-nitrophenyl)-5-(2,4-disulphophenyl)-2H-tetrazolium (CCK-8) were obtained from Aladdin Chemistry Co., Ltd. Anhydrous alcohol was obtained from Tianjin Fuyu Fine Chemical Co. Ltd. Silver nanowires (Ag) (diameter 60 nm, length 20  $\mu$ m) were produced by Shanghai Puwei Applied Materials Technology Co., Ltd. Hydrochloric acid (36–38%) was purchased from Luoyang Haohua Chemistry Co., Ltd. All reagents were of analytical grade and used as received.

### 2.2 Method

#### 2.2.1 Synthesis of TiO<sub>2</sub> nanosheets

A sample of 25 mL tetrabutyl titanate was added into a Teflon beaker containing 5 mL HF acid. After sonication for 45 min, the mixture was transferred into a Teflon-lined vessel and treated for 18 h at 200 °C, and then the as-prepared nanosheets were filtrated and washed with alcohol three times, then calcined at 550 °C in argon atmosphere for 3 h.

#### 2.2.2 Preparation of Ag/TiO<sub>2</sub>/graphene nanocomposite

The graphene oxide (GO) was prepared according to reference [31]. The Ag/TiO<sub>2</sub>/graphene nanocomposite was prepared as follows: first, a certain amount of GO was added into 50 mL deionized water and sonicated for 30 min, subsequently adding 1 mL hydrazine hydrate, TiO<sub>2</sub> nanosheets, and Ag nanowires to the GO solution with a certain ratio, and stirring to evenly disperse. Then, the mixture was transferred into a Teflon-lined vessel and reacted at 160 °C for 4 h. Finally, the product was calcined at 550 °C for 3 h under argon protection. According to their mass ratio, the TiO<sub>2</sub>/graphene foams were defined as 0.5:1, 1:1, 2:1, 3:1, or 4:1 TiO<sub>2</sub>/graphene foam (graphene to TiO<sub>2</sub>). In the main text, the 2:1 TiO<sub>2</sub>/graphene foam and the 0.15:2:1 Ag/TiO<sub>2</sub>/graphene foam were defined as TiO<sub>2</sub>/graphene and Ag/TiO<sub>2</sub>/graphene nanocomposites, respectively. The graphene foam and TiO<sub>2</sub>/graphene foam were

prepared in similar procedures in the absence of TiO<sub>2</sub> and Ag nanowires or the Ag nanowires to perform a contrast experiment, respectively.

### 3 Characterization

The Fourier-transform infrared (FT-IR) spectra of samples were characterized with a Bruker IFS66/S FT-IR spectrometer. X-ray photoelectron spectra (XPS) were measured by a PHI Quantum 2000 Scanning ESCA Microprobe system. The morphology and structure of samples were observed by field-emission scanning electron microscope (FE-SEM; HITACHI S-4800, Japan), transmission electron micrographs (TEM; FEI Tecnai G2 F20, USA), and X-ray diffraction (XRD; X'Pert-Pro MPD, Holland). The dye concentrations were determined by recording the absorbance of the solutions at 664 nm with a 722S UV–vis spectrometer at room temperature. The turbidity of *E. coli* at the optical density of 600 nm (OD<sub>600</sub>) was determined using a multi-well photometric microplate reader (Multiskan GO; Thermo Fisher Scientific, Waltham, MA, USA).

#### 3.1 Adsorption performance

In these experiments, the initial concentration of the MB solution was 30 mg/L, the pH was 7, and the adsorption experiments were performed by a shaking water bath at 200 rpm for 2 h. Typically, 10 mg adsorbing materials (TiO<sub>2</sub>, graphene foam, TiO<sub>2</sub>/graphene, or Ag/TiO<sub>2</sub>/graphene foam) was added into 100 mL MB solution. The concentrations of MB in the solutions were analyzed at 664 nm with a UV–vis spectrometer at room temperature.

#### 3.2 Photocatalytic performance

The photocatalytic performance of TiO<sub>2</sub> nanosheets, TiO<sub>2</sub>/graphene, or Ag/TiO<sub>2</sub>/graphene foam was evaluated by measuring the concentration change of MB in water under UV irradiation at room temperature. Typically, 10 mg of sample was distributed in 30 mL MB solution and stirred for 0.5 h in the dark. Then a UV lamp (500 W) with a major emission at 365 nm was placed in the center of the quartz reactor as light source. Samples (3 mL) were drawn at an interval of 10 min, and the adsorption was measured after 10 min of centrifugation (8000 rpm) with the UV–vis spectrophotometer. The degradation rate of MB was calculated according to the following equation:

$$\text{Degradation rate} = \frac{C_0 - C_t}{C_0} \times 100\% \quad (1)$$

where  $C_0$  is the initial concentration of the MB solution and  $C_t$  is the concentration of the MB solution after light irradiation time  $t$ .

After the first cycle of photocatalytic experiment, the TiO<sub>2</sub>/graphene and Ag/TiO<sub>2</sub>/graphene hybrids were collected by 10 min of centrifugation (8000 rpm) and washed by dilute HCl solution (15 wt.%) and ultrapure water three times, and then dried at 60 °C for 8 h. The dried samples were used for the next cycle of evaluation through the same procedures.

#### 3.3 Model constructing and simulation procedure

In this work, molecular dynamics (MD) simulations of the systems were carried out through the Materials Studio 8.0 software. Before assembling the composite systems, the TiO<sub>2</sub> nanoparticles, Ag nanowire, and graphene nanosheet were separately prepared geometrically optimized. Atomistic model of the TiO<sub>2</sub> nanoparticle, Ag nanowire, and graphene nanosheet for MD simulation was modeled by Materials Studio (see Fig. 1). The size of graphene nanosheet is 80 Å × 40 Å × 10 Å in length, width, and thickness, respectively. The size of TiO<sub>2</sub> nanosheet is 20 Å × 20 Å × 10 Å in length, width, and thickness, respectively. The radius of the TiO<sub>2</sub> nanosphere is 10 Å. The radius of the Ag nanowire is 6.67 Å, and the length is 80 Å. Then, the graphene, TiO<sub>2</sub> nanoparticles, or Ag nanowire was put into an empty cubic box (80 Å × 80 Å × 80 Å) to form the composite system model and geometrically optimized. After that, the composite systems were heated from 300 to 500 K and then cooled down to 300 K for 200 simulated annealing cycles. Finally, the equilibrium systems were exposed to NVT at 298 K and 1 atm for 200 ps, to obtain a fully relaxed and stable final structure, and then the interaction energy between nanoparticles was calculated. In this paper, the COMPASS force field was used in the MD simulations.

#### 3.4 Antibacterial performance

To prove the fungicide ability of samples, cell counting kit-8 (CCK-8) was used to measure *E. coli* concentration. *E. coli* in the logarithmic phase ( $2 \times 10^5$  CFU/mL) was seeded in a 96-well culture plate. Then 1 mg/mL of the samples in medium solution was added to the cell plate as the treated group, which was treated with the same conditions without samples. After treated under UV light (300 W) or under dark condition for 1 h, the cell culture medium was removed and replaced with fresh medium. Then, 10 μL CCK-8 solution was added to each culture medium and treated at 37 °C for 4 h. The absorbance at 450 nm was then recorded by a microplate reader (BIORAD, USA). Those tests were carried out and repeated three times. Cell viability was calculated from the optical density ratio of experimental cells to control cells (set to 100%).

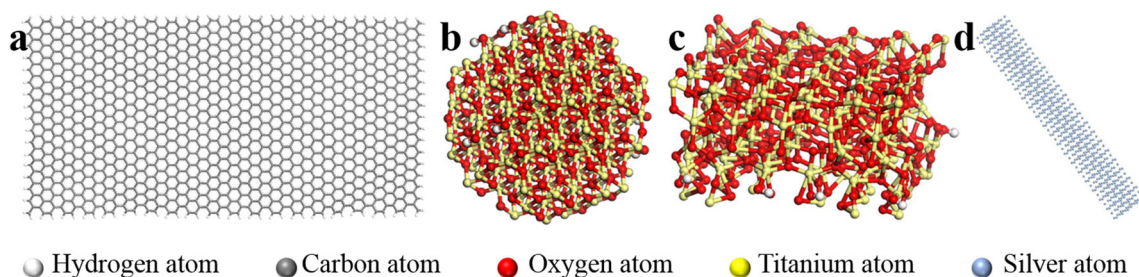


**Fig. 1** Atomistic models of (a) graphene nanosheet, (b) TiO<sub>2</sub> nanosphere, (c) TiO<sub>2</sub> nanosheet, and (d) Ag nanowire

### 4 Results and discussion

Figure 2a and e shows typical SEM and TEM images of the as-prepared TiO<sub>2</sub> nanosheets, which can be observed in abundance and regularity, with a square shape. The graphene foam shows obvious pore structure, but the graphene nanosheets aggregate obviously, which is mainly because the graphene nanosheets were extremely easy to aggregate and stack (see Fig. 2b). As shown in Fig. 2f, the graphene nanosheet exhibits a thin paper-like appearance with a large number of wrinkles. To further study the effects of the TiO<sub>2</sub> contents introduced on the foam structure, the morphologies of different composition

ratio TiO<sub>2</sub>/graphene foams were also observed by SEM. The results indicate that the foam pore density increases first and then decreases with the increase of the amount of TiO<sub>2</sub> nanosheets introduced (as shown in Fig. S1). As presented in Fig. 2c and g, the TiO<sub>2</sub> nanosheets are uniformly anchored on graphene substrate, and the 2:1 TiO<sub>2</sub>/graphene foam shows a large number of small holes and no obvious aggregation of graphene nanosheets or TiO<sub>2</sub> nanosheets is found. This phenomenon is favorable for the adsorption and photocatalytic properties of the hybrid foam. As can be seen in Fig. 2d and h, the Ag nanowires have strong attachment with graphene, which have inserted into the composite foam structure. The

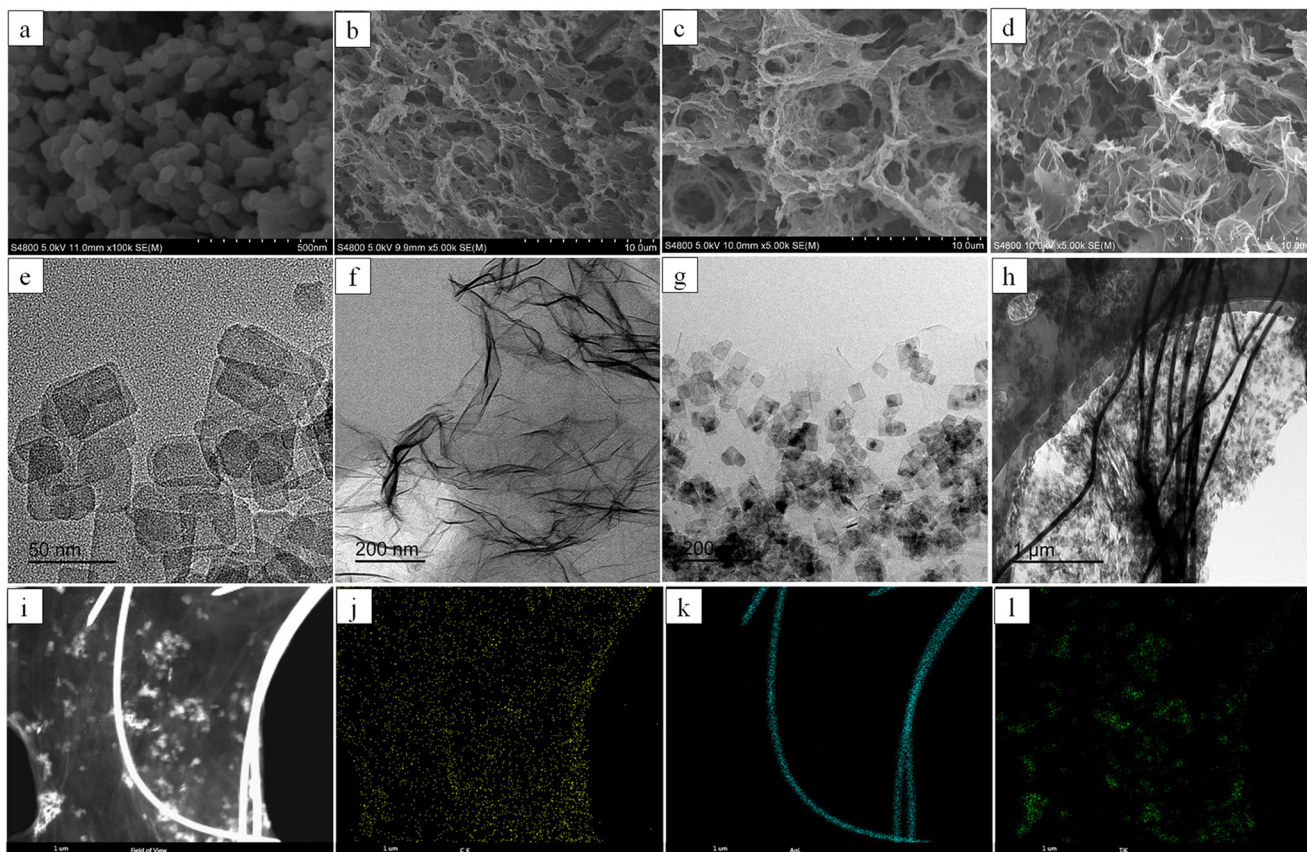


**Fig. 2** SEM and corresponding TEM images of TiO<sub>2</sub> nanosheets (a, e), graphene and its foam (b, f), 2:1 TiO<sub>2</sub>/graphene and its foam (c, g), and 0.15:2:1 Ag/TiO<sub>2</sub>/graphene nanocomposite (d, h), respectively. The

corresponding EDX area mapping (i–l) of 0.15:2:1 Ag/TiO<sub>2</sub>/graphene nanocomposite

EDX mapping (Fig. 2i–l) also provides evidence that the TiO<sub>2</sub> and the Ag nanowires are homogeneously attached on the surface of graphene.

The FT-IR spectra of GO, TiO<sub>2</sub>, TiO<sub>2</sub>/graphene, and Ag/TiO<sub>2</sub>/graphene are shown in Fig. 3. As for the GO, the absorption peaks that appear at 1056, 1638, and 3410 cm<sup>-1</sup> belonged to the stretching vibration of C–O, C=C, and –OH groups on it [32]. The characteristic peak of TiO<sub>2</sub> nanosheets appears in the range of 500 to 800 cm<sup>-1</sup>, which is assigned to bending and stretching vibrational modes of Ti–O–Ti bonds. The FT-IR spectrum of TiO<sub>2</sub>/graphene displays that the strength of C–O, C=O, and –OH groups is significantly reduced, indicating that most of the oxygen-containing functional groups on the GO surface have been removed after the hydrothermal and calcination treatment. This phenomenon confirms the successful reduction of GO to graphene [33]. The peak at 1000 cm<sup>-1</sup> belonged to the C–O stretching mode. While the measurement of XRD clearly indicates that the TiO<sub>2</sub> is highly crystallized, this phenomenon may be described as the formation of C–O–Ti bond in the TiO<sub>2</sub>/graphene system [34, 35]. The FT-IR spectrum of Ag/TiO<sub>2</sub>/graphene is similar to that of TiO<sub>2</sub>/graphene, which suggests that loading Ag nanowires will not change the chemical structure of TiO<sub>2</sub>/graphene nanocomposite.

As can be seen in Fig. 4a, the composite contains Ti, C, Ag, and O. The peaks observed at 37.0, 284.5, 367.8, 458.9, and 529.6 eV are assigned to the binding energy of Ti 3p, C 1s, Ag 3d, Ti 2p, and O 1s, respectively. The existence of Ti 3p may be due to the formation of intermetallic compounds between Ti and Ag during the process of calcination [36]. As shown in Fig. 4b, the C–C/C=C peak is almost completely overlapping the high-resolution XPS spectra of C 1s for the Ag/TiO<sub>2</sub>/graphene. This phenomenon can confirm that the GO has basically completely reduced to graphene. In Fig. 4c, two peaks at 459.3 eV (Ti 2p<sup>3/2</sup>) and 464.6 eV (Ti 2p<sup>1/2</sup>) are

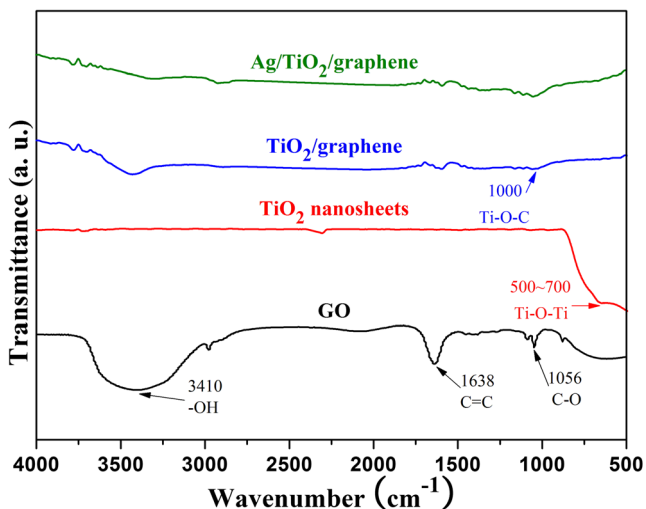


**Fig. 3** FT-IR spectra of GO, TiO<sub>2</sub>, TiO<sub>2</sub>/graphene, and Ag/TiO<sub>2</sub>/graphene

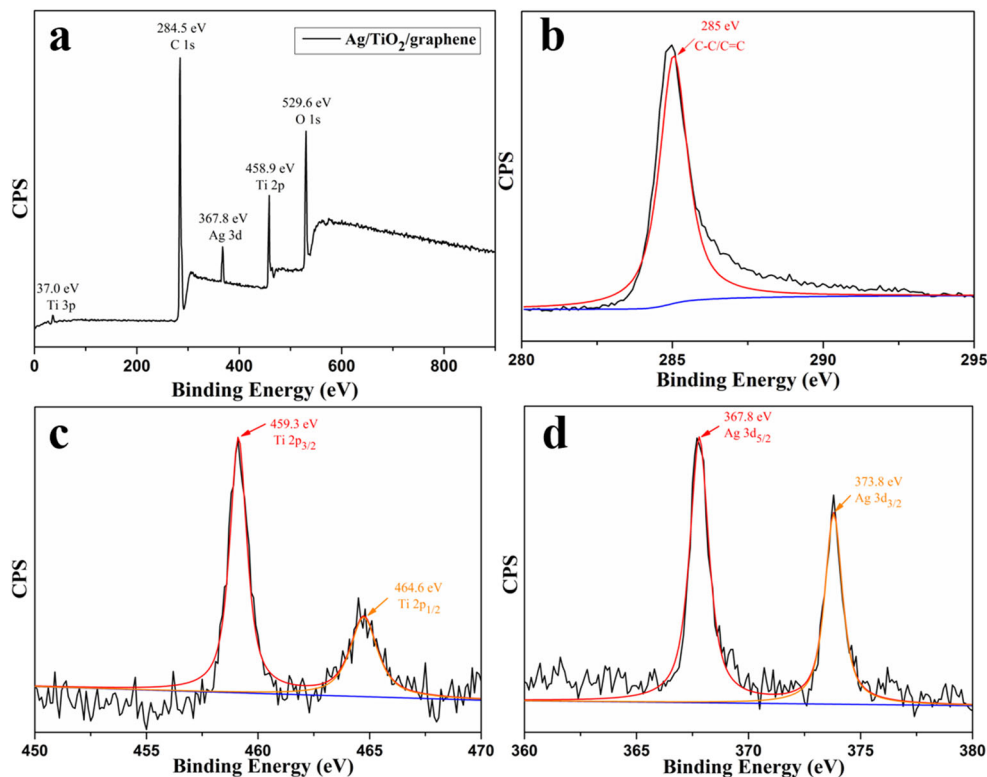
observed, which confirms the Ti in the composites existing mainly in the Ti<sup>4+</sup> state. The Ag 3d can be detected two peaks at 367.8 and 373.8 eV, which is attributed to Ag 3d<sup>5/2</sup> and Ag 3d<sup>3/2</sup>, respectively (Fig. 4d). This indicates that Ag nanowires exist in the form of zero valence elemental silver [37].

The crystal structure of the samples was characterized by XRD (as shown in Fig. 5). Graphene foam possesses a characteristic peak at  $2\theta = 24.6^\circ$ . Obviously, the patterns of TiO<sub>2</sub>/graphene are similar to those of TiO<sub>2</sub> nanosheets and no typical diffraction peaks belonging to graphene are observed. The peaks of TiO<sub>2</sub>/graphene at  $2\theta$  values of 25.3°, 37.0°, 37.9°, 38.6°, 48.1°, 53.9°, 55.1°, 62.6°, 68.8°, 70.2°, and 75.0° can be indexed to (101), (103), (004), (112), (200), (105), (211), (204), (116), (220), and (215) crystal planes of anatase TiO<sub>2</sub> [3]. This phenomenon may be attributed to the fact that depositing TiO<sub>2</sub> nanosheets on the surface of graphene can prevent its agglomeration or the characteristic peak of graphene is weak and overlaps with the (101) peak of TiO<sub>2</sub> (25.3°). Compared with that of TiO<sub>2</sub>/graphene, four additional peaks appear at 38.5°, 44.3°, 64.5°, and 77.6° in the XRD pattern of Ag/TiO<sub>2</sub>/graphene, which belonged to the (111), (200), (220), and (311) planes of face centered cubic Ag (JCPDS No. 04-0783), respectively. The results confirm that the Ag nanowires have been successfully anchored to the TiO<sub>2</sub>/graphene nanocomposite [38], while some peaks of TiO<sub>2</sub> disappear or their intensity decreases. This may be attributed to the higher intensity of Ag peaks and partly overlapped with the TiO<sub>2</sub> characteristic peaks.

It is considered that the light absorption characteristics of the catalyst are the key factors determining its photocatalytic performance. To evaluate the changes in UV absorption capacities of the TiO<sub>2</sub> and the modified TiO<sub>2</sub>, UV–vis absorption spectra of TiO<sub>2</sub>/graphene and Ag/TiO<sub>2</sub>/graphene were measured as shown in Fig. 6. As expected, the TiO<sub>2</sub> nanosheets show their photoabsorption ability in UV light region, while the TiO<sub>2</sub>/graphene and Ag/TiO<sub>2</sub>/graphene can absorb more light in the 400–800 nm region as compared with that of TiO<sub>2</sub> nanosheets. This phenomenon can define the TiO<sub>2</sub>/graphene and Ag/TiO<sub>2</sub>/graphene composites as a hybrid structure [39]. The introduction of graphene and Ag effectively broadens their light absorption range. The band gaps of TiO<sub>2</sub> nanosheets, TiO<sub>2</sub>/graphene, and Ag/TiO<sub>2</sub>/graphene composite systems are approximately 3.21, 2.8, and 2.63 eV, respectively, which are obtained from the plots of  $(\alpha h\nu)^2$  versus  $h\nu$ . This indicates that the introduction of graphene and Ag nanowires can narrow the band gap of TiO<sub>2</sub> nanosheets, thereby promoting their absorption of visible light and improving the photocatalytic efficiency. These results are in accordance with other similar reported research [40].

In this paper, MB was selected as a representative pollutant to estimate the organic pollutant removal capacity of the samples. The MB removal capacity of the samples is shown in Fig. 7. It can be seen that the TiO<sub>2</sub> nanosheets have almost no

**Fig. 4** XPS spectra of Ag/TiO<sub>2</sub>/graphene (a) and its C 1s (b), Ti 2p (c), and Ag 3d (d)



obvious adsorption capacity for MB, while the graphene foam shows great adsorption capacity to MB. As shown in Fig. S2 and Fig. S3, the adsorption and photocatalytic properties of TiO<sub>2</sub>/graphene hybrid increase continuously with the increasing of TiO<sub>2</sub> ratio under a lower introduction ratio of TiO<sub>2</sub>. Also, the TiO<sub>2</sub>/graphene (2:1) hybrid shows the best adsorption and photocatalytic properties. The enhancement of adsorption and photocatalytic properties of TiO<sub>2</sub>/graphene hybrid is mainly attributed to the high specific surface area of graphene nanosheets that can not only enhance the adsorption capacity of TiO<sub>2</sub>/graphene hybrid and provide more catalytic

active sites but also inhibit the recombination of photo-generated electrons and holes. Thus, the MB molecules can be absorbed by graphene foam and subsequently degraded by TiO<sub>2</sub> nanosheets [26, 27], while the adsorption capacity of TiO<sub>2</sub>/graphene hybrid declines when the TiO<sub>2</sub> ratio is further increased, which may be due to the fact that TiO<sub>2</sub> nanosheets have poor adsorption capacity and excessive TiO<sub>2</sub> will agglomerate to cluster on the graphene surface. This result is consistent with the results of SEM images of TiO<sub>2</sub>/graphene nanocomposite (see Fig. S1). The adsorption performance of Ag/TiO<sub>2</sub>/graphene is basically the same as that of 2:1 TiO<sub>2</sub>/

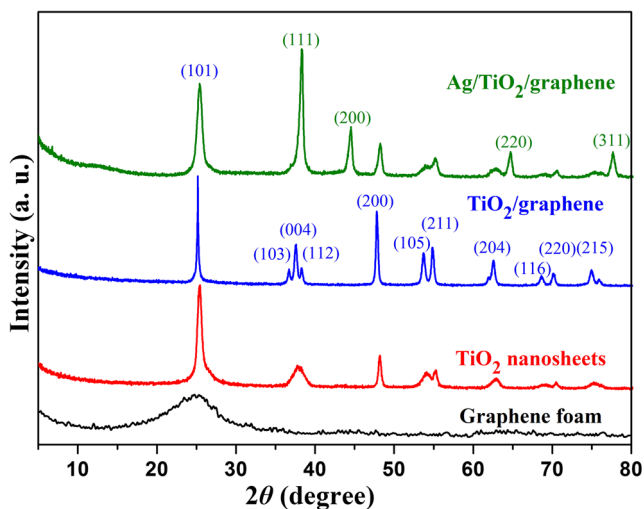


**Fig. 5** XRD patterns of the graphene foam and its derivatives

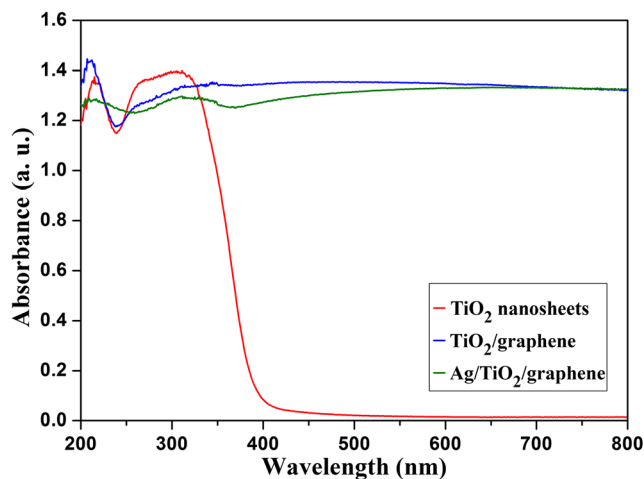


**Fig. 6** UV–vis diffuse reflectance spectra of different photocatalysts

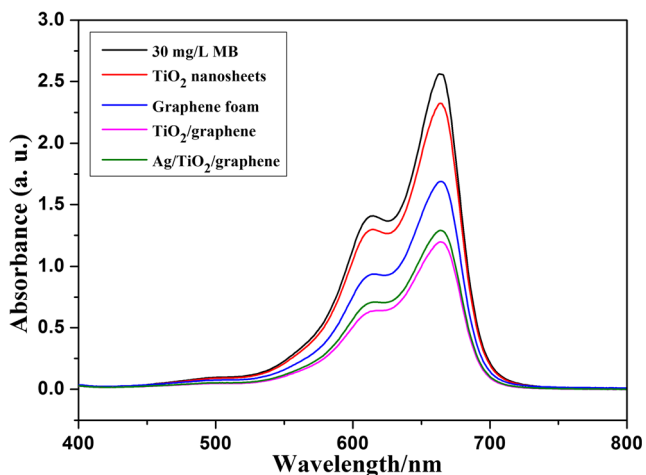


**Fig. 7** Absorption spectra of MB solution of initial concentrations 30 mg/L after treated for 2 h by different samples (10 mg) in the dark

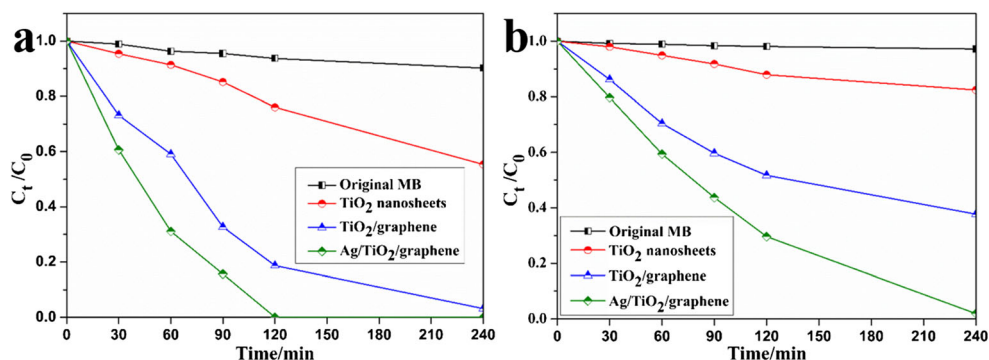
graphene, with a slight decrease (see Fig. 7). This phenomenon may be attributed to the weak adsorption capacity of Ag nanowires, which leads to the poorer adsorption capacity of Ag/TiO<sub>2</sub>/graphene than that of TiO<sub>2</sub>/graphene (2:1) hybrid under the same mass of adsorbent. In order to further study the adsorption performance of samples, 10-mg samples were placed into a disposable plastic syringe to study its adsorption and photodegradation performances on MB (30 mg/L) solution with polyvinyl chloride (PVC) foam as a separator. It can be seen in the video that the TiO<sub>2</sub>/graphene and Ag/TiO<sub>2</sub>/graphene nanocomposites show excellent ability of purifying dye wastewater (see supporting information video).

The photodegradation curves of MB under UV light and visible light irradiation is shown in Fig. 8. Compared with that of TiO<sub>2</sub> nanosheets, the TiO<sub>2</sub>/graphene and Ag/TiO<sub>2</sub>/graphene hybrids exhibit excellent photo-degradation performance. This result confirms that the introduction of graphene or Ag nanowires can effectively improve the photocatalytic activity of TiO<sub>2</sub> nanosheets. The degradation rates of TiO<sub>2</sub> nanosheets, TiO<sub>2</sub>/graphene, and Ag/TiO<sub>2</sub>/graphene to MB are 24, 82, and 100%, respectively, after 2 h of UV light irradiation, while the degradation rates of TiO<sub>2</sub> nanosheets, TiO<sub>2</sub>/graphene, and Ag/TiO<sub>2</sub>/graphene to MB are 12, 48, and 71%, respectively. Apparently, the Ag/TiO<sub>2</sub>/graphene exhibits the highest

photodegradation efficiency in the MB-contaminated water under UV light or visible light radiation.

The enhancement in photodegradation of Ag/TiO<sub>2</sub>/graphene can be attributed to three reasons [41–43]. First, graphene has a strong adsorption capacity for MB due to the strong  $\pi$ - $\pi$  interaction between them, which is helpful for the enhanced photocatalytic performance of Ag/TiO<sub>2</sub>/graphene [38]. Second, TiO<sub>2</sub> can absorb the photons with an energy comparable with its band gap and produce  $e^-$ - $h^+$  pairs. However, most of the  $e^-$ - $h^+$  pairs will recombine quickly without any effect. For most anatase-type TiO<sub>2</sub>, its conduction band (CB) is located at -4.21 eV with energy gap amplitude of 3.2 eV. Pristine graphene has a work function of 4.42–4.66 eV. Due to the incomplete reduction, the work function of GO is generally higher than that of graphene. Therefore, the photo-generated  $e^-$  can be transferred to graphene avoiding the recombination with the valence band (VB) holes [44]. Some studies have reported that the Ag<sup>+</sup> can be reduced in graphene/TiO<sub>2</sub> composite system. This indicates that the energy level of the anti-bond  $\pi^*$  orbital is higher than that of Ag, and thus the  $e^-$  can be conducted from graphene to Ag<sup>+</sup>. It can be concluded that  $e^-$  can be injected into Ag nanowires from graphene in an excited state [45]. Graphene acts as  $e^-$  transfer medium during the photocatalytic reaction. The work function of Ag is 4.26 eV. When TiO<sub>2</sub> nanosheets come into contact with the Ag nanowires, a Schottky barrier will form at their interface. These will improve the separation efficiency of  $e^-$ - $h^+$  pairs and prevent their recombination, thus increasing the photocatalytic activity of Ag/TiO<sub>2</sub>/graphene [46]. Since the excited MB has a lower work function (3.81 eV) than graphene and lying above the CB of TiO<sub>2</sub>, it can also transfer  $e^-$  to TiO<sub>2</sub> and graphene. The  $e^-$  transfer efficiency is mainly related to the contact between graphene and TiO<sub>2</sub>. TiO<sub>2</sub> nanosheets have a larger contact area with graphene than that of TiO<sub>2</sub> nanospheres, thereby effectively improving the separation efficiency of  $e^-$  and  $h^+$  [47]. The produced  $e^-$  can react with the O<sub>2</sub> absorbed on the surface of TiO<sub>2</sub> nanosheets (or graphene and Ag nanowires) and form superoxide anions ( $\cdot\text{O}_2^-$ ). Both  $h^+$  and the produced  $\cdot\text{O}_2^-$  can react with H<sub>2</sub>O to generate  $\cdot\text{OH}$  radicals. The  $\cdot\text{OH}$  radicals can degrade organic pollutants into CO<sub>2</sub> and H<sub>2</sub>O (as shown in Fig. 9). Third, the

**Fig. 8** Photocatalytic degradation of MB (30 mg/L) in the presence of different samples (10 mg) under UV light (a) and visible light (b) irradiation



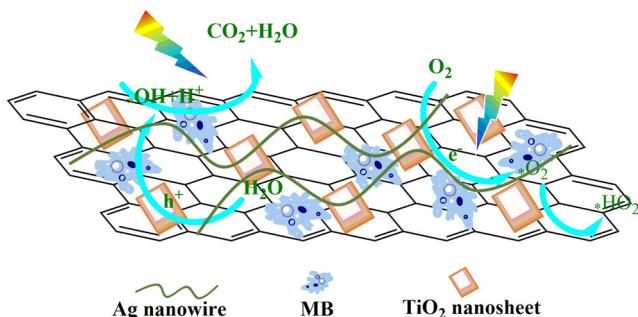
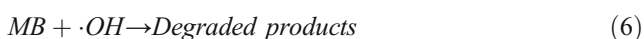
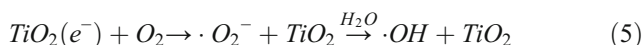
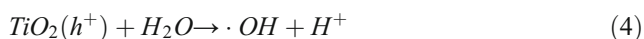
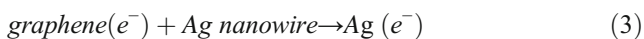


**Fig. 9** The hypothetical mechanism of Ag/TiO<sub>2</sub>/graphene for photodegradation reaction

unique 3D foam structure can not only effectively hold its large specific surface area by avoiding the stack of graphene nanosheets but also minimize the reflection of incident light and improve the light utilization efficiency. Such efficient synergy between the adsorption of graphene, photocatalytic performance of TiO<sub>2</sub>, and the unique 3D structure results in efficient MB degradation by the Ag/TiO<sub>2</sub>/graphene foam [48]. The possible degradation mechanism of MB by Ag/TiO<sub>2</sub>/graphene under light illumination is presented as follows. This may require further experiments and characterization in the future to verify it.



Loading TiO<sub>2</sub> on the graphene surface can highly improve the photocatalytic performance of TiO<sub>2</sub> nanoparticles, and the degree of improvement and stability of composite catalyst are closely related to the combination of graphene and TiO<sub>2</sub> nanoparticles. The combination between TiO<sub>2</sub> and graphene can be evaluated by their binding energy. The larger the binding energy, the more energy is needed to destroy the interface of their composite structure, and the more stable the composite structure will be [28]. The interface regions of TiO<sub>2</sub>/graphene, Ag/graphene, or Ag/TiO<sub>2</sub>/graphene (as can be seen in Fig. 10) systems are simulated for studying its interfacial bonding force by molecular dynamics simulation under COMPASS force fields. The interaction energy ( $E_{int}$ ) between graphene and TiO<sub>2</sub> nanoparticle (or Ag nanowire) can be calculated by Eq. 7 [29]:

$$E_{inter} = -(E_{total} - E_{graphene} - E_{TiO_2 \text{ (or Ag)}}) \quad (7)$$

where  $E_{total}$  is the total potential energy of TiO<sub>2</sub>/graphene or Ag/graphene,  $E_{graphene}$  is the potential energy of graphene,  $E_{TiO_2}$  is the potential energy of TiO<sub>2</sub> nanosheet (or TiO<sub>2</sub> nanosphere), and  $E_{Ag}$  is the potential energy of graphene.

It can be seen in Fig. 10a that the TiO<sub>2</sub> nanosphere is adsorbed on the edge of the graphene surface. As shown in Fig. 10b, the graphene is curled around the TiO<sub>2</sub> nanosheet. This phenomenon may be due to the stronger interaction between graphene and TiO<sub>2</sub> nanosheet than that between graphene and TiO<sub>2</sub> nanosphere. In Fig. 10c, the Ag nanowire is tightly attached to the surface of graphene. Even in the Ag/TiO<sub>2</sub>/graphene composite system, one end of the Ag nanowire remains tightly attached to the graphene surface. Meanwhile, the  $E_{int}$  between TiO<sub>2</sub> nanosheet and graphene is calculated as  $-965.17 \text{ kcal/mol}$ , far above the  $E_{int}$  between TiO<sub>2</sub> nanosphere and graphene ( $-392.44 \text{ kcal/mol}$ ). The  $E_{int}$  between Ag nanowire and graphene is calculated as  $-624.32 \text{ kcal/mol}$ . It can be concluded that the TiO<sub>2</sub> nanosheets/graphene composite catalyst has better microstructure stability than that of TiO<sub>2</sub> nanospheres/graphene composite catalyst. Also, the stability of Ag/TiO<sub>2</sub>/graphene foam structure is good.

MB photodegradation leads to a decrease in its absorbance value, which is considered to be a sign of MB degradation. In order to study the intermediates in the degradation process and explore the pathway of MB photodegradation, GC-MS analysis technique was used for identification in the presence of Ag/TiO<sub>2</sub>/graphene foam. As seen in Fig. 11a, the high intensity single peak at  $m/z = 284$  is assigned to the molecular ion peak for MB. While after 30 min of irradiation under UV light, the peak intensity at  $m/z = 284$  has significantly reduced and the appearance of new peaks is attributed to the intermediate products shown in Fig. 11b. Initially, the oxidation of the sulfur to sulfone, hydroxylation of phenyl rings, and *N*-methyl groups of MB leads to the products with  $m/z$  396 and  $m/z$  354. The possibility of being attacked by active  $\cdot OH$  to form sulfone has been confirmed by researchers [49]. Then, the photo-generated holes, hydroxyl radicals, and hydroperoxide radicals formed during photodegradation preferentially attack the chromophore center of the dye molecule. The imino group cleavage and its saturation by the hydrogen radical, the demethylation cleavage, and release of one or more of the methyl group substituents on the amine groups and further oxidation lead to the formation of the products with  $m/z$  270,  $m/z$  241,  $m/z$  219, and  $m/z$  153. With further extension of UV irradiation time, the further attack of active radical on the aromatic rings activate them and follow on the generation of more main byproducts ( $m/z$  230,  $m/z$  201,  $m/z$  135,  $m/z$  125,  $m/z$  99, and  $m/z$  59). As shown in Fig. 11d, the intensity of peaks at  $m/z$  256,  $m/z$  270, and  $m/z$  241 decreases as the time increases, and eventually disappears completely. These results may be attributed to the decomposition of the aromatic ring, and the resulting smaller intermediates subsequently undergo continuous degradation reactions to produce carbon dioxide, water, ammonium, and sulfate ions. Based on the determination of intermediate products, a possible degradation pathway of MB by the Ag/TiO<sub>2</sub>/graphene foam system is proposed, as demonstrated in Fig. 12.



**Fig. 10** Molecular model of the interface region in TiO<sub>2</sub>/graphene composites. **a** TiO<sub>2</sub> nanosphere/graphene, **b** TiO<sub>2</sub> nanosheet/graphene, **c** Ag nanowire/graphene, and **d** Ag nanowire/TiO<sub>2</sub> nanosheet/graphene

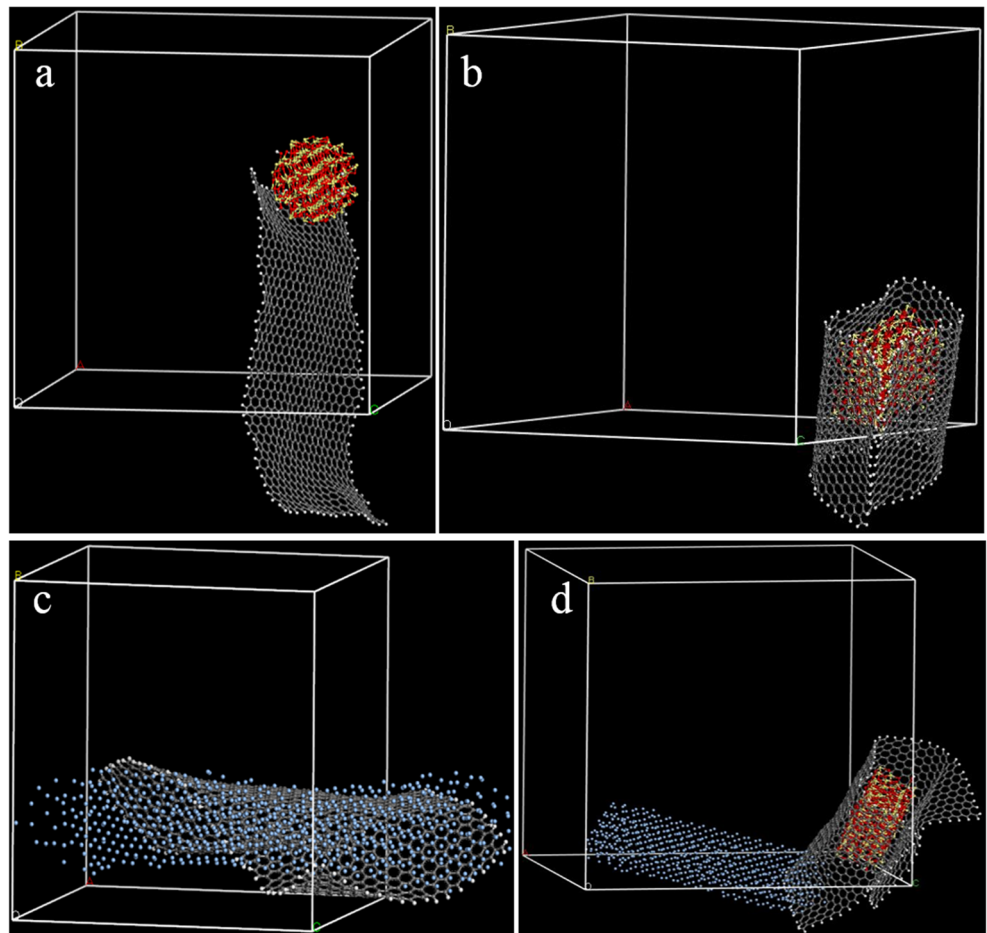


**Fig. 11** GC-MS spectra of the MB (30 mg/L) photocatalytic degradation products in the presence of Ag/TiO<sub>2</sub>/graphene (10 mg) under UV light irradiation for 0 min (**a**), 30 min (**b**), 90 min (**c**), and 240 min (**d**), respectively

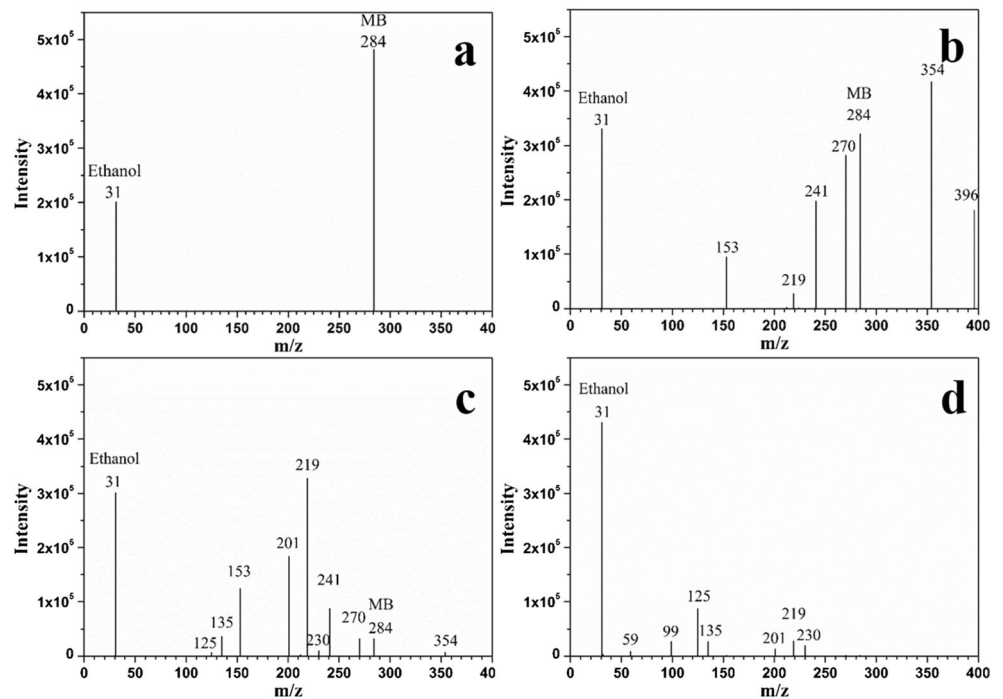


**Fig. 12** Proposed degradation reaction mechanism of MB by Ag/TiO<sub>2</sub>/graphene

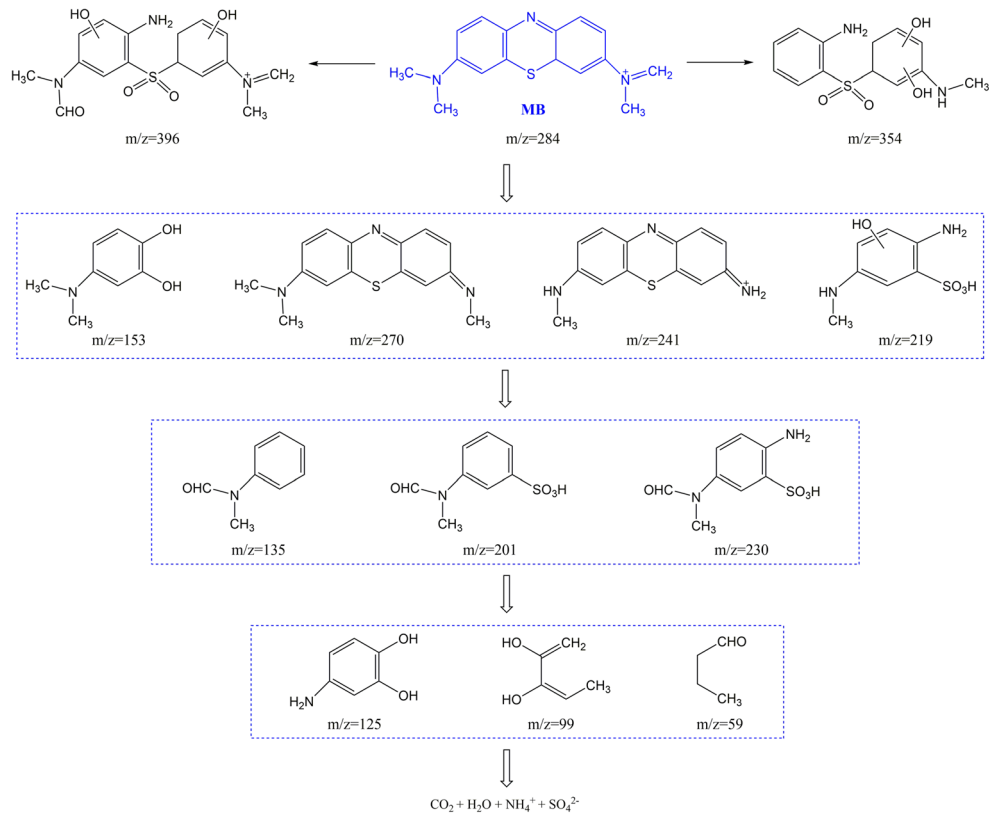
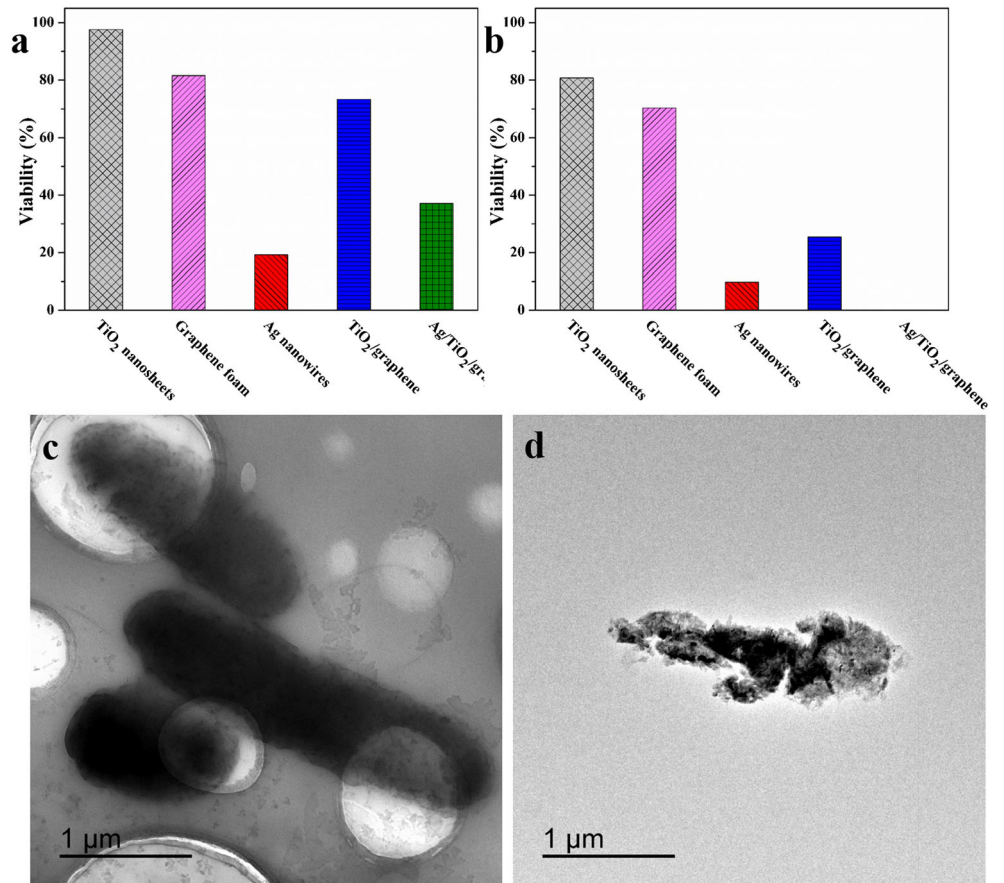


**Fig. 13** The viability of *E. coli* treated for 1 h with different samples under dark (a) and UV light (b) condition; TEM images of the untreated (c) and treated (d) *E. coli*



As can be seen in Fig. 13a, the TiO<sub>2</sub> nanosheets barely affect the viability of *E. coli* under dark condition. However, the viability of *E. coli* is significantly reduced when it is incubated with Ag nanowires or Ag/TiO<sub>2</sub>/graphene nanocomposite in the dark for 1 h due to the intrinsic antibacterial properties of the Ag nanowires and graphene. Figure 13b shows that the viability reduces obviously when the three systems are exposed to UV light for 1 h. Especially for the Ag/TiO<sub>2</sub>/graphene nanocomposite, the viability of *E. coli* decreases to 0%. These may be attributed to a large amount of reactive oxygen species (ROS) generation that can kill the bacteria [50]. At the same time, the bactericidal activity of graphene foam and Ag nanowires to *E. coli* under UV irradiation is significantly stronger than those under dark condition, which may be related to the certain bactericidal activity of UV light against bacteria. Furthermore, the TEM was used to study the morphological changes of typical *E. coli* before and after exposing to UV light. As shown in Fig. 13c, the live *E. coli* have a smooth surface and with regular rod-like shapes. However, obvious cell damages can be observed for the bacteria as shown in Fig. 13d, in which the regular rod-like shapes have disappeared after treatment by Ag/TiO<sub>2</sub>/graphene system. It can be concluded that *E. coli* has been completely inactivated, making the treated water safe to use. The excellent bactericidal activity of Ag/TiO<sub>2</sub>/graphene is mainly attributed to the synergistic effect of Ag, TiO<sub>2</sub>, and graphene. The released Ag<sup>+</sup> in the system interacts with cell and causes cell death by different approaches [51, 52]. The modified TiO<sub>2</sub> nanosheets can produce ROS that damage the cell membranes under UV light stimulation. Also, the high-surface-area graphene nanosheets can adsorb and gather the *E. coli* onto its surface, thereby enhancing the efficiency of interaction between bacteria and active germicidal components [53].

Recyclability is critical to the practical application of the catalyst. So, recycle testing of the prepared samples was also investigated. The typical cycling experiments of TiO<sub>2</sub>/graphene and Ag/TiO<sub>2</sub>/graphene are conducted to evaluate their long-term serving life, and the results are shown in Fig. 14. The results show that their photocatalytic efficiency has not exhibited significant loss after 5 cycles (see Fig. 14). This phenomenon can be explained as that the TiO<sub>2</sub>/graphene and Ag/TiO<sub>2</sub>/graphene can degrade the MB molecules adsorbed by graphene nanosheets, so that the surface of graphene nanosheets has open spaces for MB molecules, and the adsorption process can be repeated continuously, while the Ag/TiO<sub>2</sub>/graphene shows more stable cycle property than TiO<sub>2</sub>/graphene, which may be attributed to Ag/TiO<sub>2</sub>/graphene having more excellent photocatalytic properties, thereby facilitating the removal of adsorbates on its surface. This phenomenon also confirms that the Ag/TiO<sub>2</sub>/graphene has excellent photochemical stability. From the perspective of practical application, the aforementioned results are of great significance because increasing the photocatalytic activity and preventing catalyst deactivation will make the application more economical and effective.

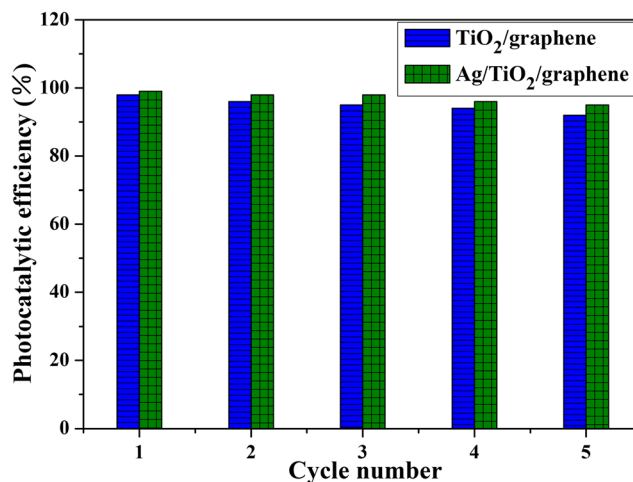


Fig. 14 Recycle tests of MB removal by TiO<sub>2</sub>/graphene and Ag/TiO<sub>2</sub>/graphene

## 5 Conclusion

In summary, a novel Ag/TiO<sub>2</sub>/graphene hybrid foam was successfully synthesized by coupling Ag nanowires and graphene with TiO<sub>2</sub> nanosheets, and used as adsorbent and photocatalyst for water treatment. Compared with the pristine TiO<sub>2</sub> and graphene foam, the Ag/TiO<sub>2</sub>/graphene hybrid foam demonstrated much higher adsorption capacity, photocatalytic activity, and bactericidal activity. Its superior water treatment performance was attributed to the high transport nature of the porous foam structure, effective structural composition, and effectively promoting the separation of photo-generated  $e^- - h^+$  pairs. Furthermore, good recycle stability of Ag/TiO<sub>2</sub>/graphene nanocomposite has great potential application in water treatment. The synergistic interactions between the Ag, graphene, and TiO<sub>2</sub> provided a robust and novel method for combining the materials with different properties to obtain a water treatment agent with excellent comprehensive performance. Meanwhile, this study provides some new insights into the design and fabrication of advanced water treatment agents with foam structures toward highly efficient photocatalytic applications in organic pollution treatment and sterilization under light irradiation.

**Acknowledgments** This work was supported by the Natural Science Basic Research Plan in Shaanxi Province of China (Program No. 2018JQ5211), National Key Research and Development Program of China (No. 2017YFB0308602), and the Special Scientific Research Program Founded by Shaanxi Provincial Education Department (No. 18JK0102).

## Compliance with ethical standards

**Conflict of interest** The authors declare that they have no conflicts of interest.

## References

- Choi JU, Kim YG, Jo WK (2019) Multiple photocatalytic applications of non-precious Cu-loaded g-C<sub>3</sub>N<sub>4</sub>/hydrogenated black TiO<sub>2</sub> nanofiber heterostructure. *Appl Surf Sci* 473:761–769
- Cai CY, Zhao MH, Yu Z, Rong HW, Zhang CS (2019) Utilization of nanomaterials for in-situ remediation of heavy metal (loid) contaminated sediments: a review. *Sci Total Environ* 662:205–217
- Bao Y, Kang QL, Liu C, Ma JZ (2018) Sol-gel-controlled synthesis of hollow TiO<sub>2</sub> spheres and their photocatalytic activities and lithium storage properties. *Mater Lett* 214:272–275
- Bi JT, Huang X, Wang JK, Wang T, Wu H, Yang JY, Lu HJ, Hao HX (2019) Oil-phase cyclic magnetic adsorption to synthesize Fe<sub>3</sub>O<sub>4</sub>@C@TiO<sub>2</sub>-nanotube composites for simultaneous removal of Pb (II) and Rhodamine B. *Chem Eng J* 366:50–61
- Surowka M, Kobielusz M, Trochowski M, Buchalska M, Kruczała K, Bros P, Macyk W (2019) Iron and other metal species as phase-composition controllers influencing the photocatalytic activity of TiO<sub>2</sub> materials. *Appl Catal B Environ* 247:173–181
- Chen XB, Liu L, Yu PY, Mao SS (2011) Increasing solar absorption for photocatalysis with black hydrogenated titanium dioxide nanocrystals. *Science* 331(6018):746–750
- Bai X, Jia J, Du YY, Hu XY, Li JL, Liu EZ, Fan J (2020) Multi-level trapped electrons system in enhancing photocatalytic activity of TiO<sub>2</sub> nanosheets for simultaneous reduction of Cr(VI) and RhB degradation. *Appl Surf Sci* 503:144298
- Liu C, Dong YF, Lin Y, Yan HX, Zhang WB, Bao Y, Ma JZ (2019) Enhanced mechanical and tribological properties of graphene/bismaleimide composites by using reduced graphene oxide with non-covalent functionalization. *Compos Part B* 165:491–499
- Huangfu YM, Liang CB, Han YX, Qiu H, Song P, Wang L, Kong J, Gu JW (2019) Fabrication and investigation on the Fe<sub>3</sub>O<sub>4</sub>/thermally annealed graphene aerogel/epoxy electromagnetic interference shielding nanocomposites. *Compos Sci Technol* 169:70–75
- Ruan KP, Guo YQ, Tang YS, Zhang YL, Zhang JN, He MK, Kong J, Gu JW (2018) Improved thermal conductivities in polystyrene nanocomposites by incorporating thermal reduced graphene oxide via electrospinning-hot press technique. *Compos Commun* 10:68–72
- Wang H, Zhu KY, Yan LW, Wei C, Zhang Y, Gong CH, Guo JH, Zhang JW, Zhang DM, Zhang JW (2019) Efficient and scalable high-quality graphene nanodot fabrication through confined lattice plane electrochemical exfoliation. *Chem Commun* 55(41):5805–5808
- Singh N, Jana S, Singh GP, Dey RK (2020) Graphene-supported TiO<sub>2</sub>: study of promotion of charge carrier in photocatalytic water splitting and methylene blue dye degradation. *Adv Compos Hybrid Mater* 3:127–140
- Konicki W, Aleksandrak M, Moszyński D, Mijowska E (2017) Adsorption of anionic azo-dyes from aqueous solutions onto graphene oxide: equilibrium, kinetic and thermodynamic studies. *J Colloid Interface Sci* 496:188–200
- Yang KJ, Wang J, Chen XX, Zhao Q, Ghaffar A, Chen BL (2018) Application of graphene-based materials in water purification: from the nanoscale to specific devices. *Environ Sci-Nano* 5(6):1264–1297
- Kanjwal MA, Lo KKS, Leung WWF (2019) Graphene composite nanofibers as a high-performance photocatalyst for environmental remediation. *Sep Purif Technol* 215:602–611
- Kadi MW, Mohamed RM (2019) Preparation and characterization of Pt, N-TiO<sub>2</sub>-graphene nanocomposites for hydrogen production. *Ceram Int* 45(5):6058–6065
- Zhu MS, Chen PL, Liu MH (2011) Graphene oxide enwrapped Ag/AgX (X = Br, Cl) nanocomposite as a highly efficient visible-light plasmonic photocatalyst. *ACS Nano* 5(6):4529–4536
- Zhang L, Qi HJ, Zhao Y, Zhong LL, Zhang YJ, Wang Y, Xue JQ, Li Y (2019) Au nanoparticle modified three-dimensional network PVA/RGO/TiO<sub>2</sub> composite for enhancing visible light photocatalytic performance. *Appl Surf Sci* 498:143855
- Sreeja S, Shetty KV (2016) Microbial disinfection of water with endotoxin degradation by photocatalysis using Ag@TiO<sub>2</sub> core shell nanoparticles. *Environ Sci Pollut Res* 23(18):18154–18164
- Zhao HL, Deng W, Li Y (2018) Atomic layer deposited TiO<sub>2</sub> ultrathin layer on Ag\_ZnO nanorods for stable and efficient photocatalytic degradation of RhB. *Adv Compos Hybrid Mater* 1:404–413
- Qin M, Chang Q, Yu YK, Wu HJ (2019) Exterior and internal uniform loading of Pt nanoparticles on yolk-shell La<sub>2</sub>O<sub>3</sub> by acoustic levitation synthesis with enhanced photocatalytic performance. *Materials* 13(1):107
- Zhao ZH, Liu JL, Gong H, Wu GL, Wu HJ (2019) Pt/Ni<sub>0.17</sub>Zn<sub>0.83</sub>O hybrids with enhanced photocatalytic performance: effect of reduction treatments. *Results Phys* 14:102434
- Liu HY, Liang C, Niu CG, Huang DW, Du YB, Guo H, Zhang L, Yang YY, Zeng GM (2019) Facile assembly of g-C<sub>3</sub>N<sub>4</sub>/Ag<sub>2</sub>CO<sub>3</sub>/graphene oxide with a novel dual Z-scheme system for enhanced photocatalytic pollutant degradation. *Appl Surf Sci* 475:421–434
- Zhao ZH, Liu JL, Qin M, Kou KC, Wu GL, Wu HJ (2020) Effective cocatalyst Pt/PtO nanodots on La<sub>2</sub>O<sub>3</sub> microspheres for degradation of methyl orange. *J Nanosci Nanotechnol* 20(5):3140–3147
- Wang Q, Cai CY, Wang MY, Guo Q, Wang B, Luo WN, Wang YJ, Zhang CY, Zhou LH, Zhang DE (2018) Efficient photocatalytic degradation of malachite green in seawater by the hybrid of zinc-oxide nanorods grown on three-dimensional (3D) reduced graphene oxide (RGO)/Ni foam. *Materials* 11(6):1004
- Liu WH, Gao Y, Yang YP, Zou Q, Yang GX, Zhang ZP, Li HF, Miao YC, Li HX, Huo YN (2018) Photocatalytic composite of a floating BiOBr@graphene oxide@melamine foam for efficient removal of organics. *Chemcatchem* 10(11):2394–2400
- Wang XY, Wang HH, Yu K, Hu XF (2018) Immobilization of 2D/2D structured g-C<sub>3</sub>N<sub>4</sub> nanosheet/reduced graphene oxide hybrids on 3D nickel foam and its photocatalytic performance. *Mater Res Bull* 97:306–313
- Men XJ, Chen HB, Chang KW, Fang XF, Wu CF, Qin WP, Yin SY (2016) Three-dimensional free-standing ZnO/graphene composite foam for photocurrent generation and photocatalytic activity. *Appl Catal B Environ* 187:367–374
- Cao F, Wang T, Ji XH (2019) Enhanced visible photocatalytic activity of tree-like ZnO/CuO nanostructure on Cu foam. *Appl Surf Sci* 471:417–424
- Reli M, Troppova I, Sihor M, Pavlovsky J, Praus P, Koci K (2019) Photocatalytic decomposition of N<sub>2</sub>O over g-C<sub>3</sub>N<sub>4</sub>/BiVO<sub>4</sub> composite. *Appl Surf Sci* 469:181–191
- Kovtyukhova NI, Ollivier PJ, Martin BR, Mallouk TE, Chizhik SA, Buzaneva EV, Gorchinskiy AD (1999) Layer-by-layer assembly of ultrathin composite films from micron-sized graphite oxide sheets and polycations. *Chem Mater* 11(3):771–778
- Liu C, Yan HX, Lv Q, Li S, Niu S (2016) Enhanced tribological properties of aligned reduced graphene oxide-Fe<sub>3</sub>O<sub>4</sub>@polyphosphazene/bismaleimides composites. *Carbon* 102:145–153
- Zhang LX, Ni CH, Jiu HF, Xie CM, Yan JB, Qi GS (2017) One-pot synthesis of Ag-TiO<sub>2</sub>/reduced graphene oxide nanocomposite for high performance of adsorption and photocatalysis. *Ceram Int* 43(7):5450–5456
- Nasrollahzadeh M, Atarod M, Jaleh B, Gandomirouzbahani M (2016) In situ green synthesis of Ag nanoparticles on graphene oxide/TiO<sub>2</sub> nanocomposite and their catalytic activity for the reduction of 4-nitrophenol, Congo red and methylene blue. *Ceram Int* 42(7):8587–8596
- Zhao J, Zhang JL, Wang L, Lyu SS, Ye WL, Xu BB, Qiu H, Chen LX, Gu JW (2020) Fabrication and investigation on ternary

- heterogeneous MWCNT@TiO<sub>2</sub>-C fillers and their silicone rubber wave-absorbing composites. *Compos A Appl Sci Manuf* 129: 105714
36. Zhao LN, Jia YH, You H, Wang ST, Fu L (2020) Photocatalytic performance and application outlook of 3D TiO<sub>2</sub>/titanium mesh modified by GO-Ag joined-deposition. *Catal Today* 340:106–114
  37. Zou J, Mao DP, Wee ATS, Jiang JZ (2019) Micro/nano-structured ultrathin g-C<sub>3</sub>N<sub>4</sub>/Ag nanoparticle hybrids as efficient electrochemical biosensors for L-tyrosine. *Appl Surf Sci* 467:608–618
  38. Wen YY, Ding HM, Shan YK (2011) Preparation and visible light photocatalytic activity of Ag/TiO<sub>2</sub>/graphene nanocomposite. *Nanoscale* 3(10):4411–4417
  39. Zhao L, Chen XF, Wang XC, Zhang YJ, Wei W, Sun YH, Antonietti M, Titirici MM (2010) One-step solvothermal synthesis of a carbon@TiO<sub>2</sub> dyade structure effectively promoting visible-light photocatalysis. *Adv Mater* 22(30):3317–3321
  40. Neațu S, Macia-Agullo JA, Concepcion P, Garcia H (2014) Gold-copper nanoalloys supported on TiO<sub>2</sub> as photocatalysts for CO<sub>2</sub> reduction by water. *J Am Chem Soc* 136(45):15969–15976
  41. Kumbhakar P, Pramanik A, Biswas S, Kole AK, Sarkar R, Kumbhakar P (2018) In-situ synthesis of rGO-ZnO nanocomposite for demonstration of sunlight driven enhanced photocatalytic and self-cleaning of organic dyes and tea stains of cotton fabrics. *J Hazard Mater* 360:193–203
  42. Liu X, Xu X, Sun J, Alsaedi A, Hayat T, Li J, Wang X (2018) Insight into the impact of interaction between attapulgite and graphene oxide on the adsorption of U (VI). *Chem Eng J* 343: 217–224
  43. Higgins D, Hoque MA, Seo MH, Wang RY, Hassan F, Choi JY, Pritzker M, Yu AP, Zhang JJ, Chen ZW (2014) Development and simulation of sulfur-doped graphene supported platinum with exemplary stability and activity towards oxygen reduction. *Adv Funct Mater* 24(27):4325–4336
  44. Qi HP, Wang HL, Zhao DY, Jiang WF (2019) Preparation and photocatalytic activity of Ag-modified GO-TiO<sub>2</sub> mesocrystals under visible light irradiation. *Appl Surf Sci* 480:105–114
  45. Beasley C, Gnanamani MK, Santillan-Jimenez E, Martinelli M, Shafer WD, Hopps SD, Wanninayake N, Kim DY (2020) Effect of metal work function on hydrogen production from photocatalytic water splitting with MTiO<sub>2</sub> catalysts. *ChemistrySelect* 5(3):1013–1019
  46. Yu HL, Wu QX, Wang J, Liu LQ, Zheng B, Zhang C, Shen YG, Huang CL, Zhou B, Jia JR (2020) Simple fabrication of the Ag-Ag<sub>2</sub>O-TiO<sub>2</sub> photocatalyst thin films on polyester fabrics by magnetron sputtering and its photocatalytic activity. *Appl Surf Sci* 503: 144075
  47. Xiang XM, Pan FP, Li Y (2018) A review on adsorption-enhanced photoreduction of carbon dioxide by nanocomposite materials. *Adv Compos Hybrid Mater* 1:6–31
  48. Yang XT, Fan SG, Li Y, Guo YQ, Li YG, Ruan KP, Zhang SM, Zhang JL, Kong J, Gu JW (2020) Synchronously improved electromagnetic interference shielding and thermal conductivity for epoxy nanocomposites by constructing 3D copper nanowires/thermally annealed graphene aerogel framework. *Compos A Appl Sci Manuf* 128:105670
  49. Kshirsagar AS, Gautam A, Khanna PK (2017) Efficient photocatalytic oxidative degradation of organic dyes using CuInSe<sub>2</sub>/TiO<sub>2</sub> hybrid hetero-nanostructures. *J Photochem Photobiol A Chem* 349:73–90
  50. Li WL, Li BR, Meng MJ, Cui YH, Wu YL, Zhang YL, Dong HJ, Feng YH (2019) Bimetallic au/Ag decorated TiO<sub>2</sub> nanocomposite membrane for enhanced photocatalytic degradation of tetracycline and bactericidal efficiency. *Appl Surf Sci* 487:1008–1017
  51. Noreen Z, Khalid NR, Abbasi R, Javed S, Ahmad I, Bokhari H (2019) Visible light sensitive Ag/TiO<sub>2</sub>/graphene composite as a potential coating material for control of *Campylobacter jejuni*. *Mater Sci Eng C* 98:125–133
  52. Liang CB, Song P, Qiu H, Zhang YL, Ma XT, Qi FQ, Gu HB, Kong J, Cao DP, Gu JW (2019) Constructing interconnected spherical hollow conductive networks in silver platelets/reduced graphene oxide foam/epoxy nanocomposites for superior electromagnetic interference shielding effectiveness. *Nanoscale* 11(46):22590–22598
  53. Yang XF, Qin JL, Jiang Y, Li R, Li Y, Tang H (2014) Bifunctional TiO<sub>2</sub>/Ag<sub>3</sub>PO<sub>4</sub>/graphene composites with superior visible light photocatalytic performance and synergistic inactivation of bacteria. *RSC Adv* 4(36):18627–18636

**Publisher's note** Springer Nature remains neutral with regard to jurisdictional claims in published maps and institutional affiliations.